Science Advances

AAAS

advances.sciencemag.org/cgi/content/full/4/5/eaas8652/DC1

Supplementary Materials for

Making data matter: Voxel printing for the digital fabrication of data across scales and domains

Christoph Bader, Dominik Kolb, James C. Weaver, Sunanda Sharma,
Ahmed Hosny, João Costa, Neri Oxman

Published 30 May 2018, *Sci. Adv.* **4**, eaas8652 (2018)
DOI: 10.1126/sciadv.aas8652

This PDF file includes:

Supplementary Information

Limitations of Boundary Representations in 3D Printing Workflows

Here we describe two examples of current limitations of 3D printing workflows illustrating the points made in the main text.

Figure S1 illustrates the traditional conversion process of white matter tractography data of a human brain. The fiber data that is rendered on screen is represented through 5,721 individual colored polygon chains with a total of 625,078 vertices. In order to 3D print this data set with conventional methods, a 3D strut algorithm can be used that creates a tubular enclosure for every polygon chain. The resulting STL file is represented though 6,250,780 vertices, which increases the vertex count of the new data set by a factor of 10, compared to original file. Furthermore the color information that is stored in the newly created strut structure can't be directly imported into the printing software of modern multimaterial 3D printers. A workaround for this problem is the use of an additional color texture that some of the printer software can read. But regarding the size of the strut file, the process of texture mapping and transferring vertex colors to a dedicated texture map is inconvenient and creates further computational overhead.

Figure S2 shows another example of a scientific data set that is particularly difficult to additively manufacture with common 3D printing workflows. The data represents volumetric information in the form of an image stack that is captured through protein-retention expansion microscopy (*30*). One possible workflow of additively manufacturing such data, for example, would require the image stack to be initially converted into a three-dimensional volumetric data structure, where every image pixel is mapped to a volume voxel. Since each image of the stack has a resolution of 2316 px × 1901 px, the resulting volume with a height of 460px consists of 2 billion voxels, which makes any processing on this high-resolution data set computationally intensive or even impossible. The next step would involve the generation of an STL file through isosurface extraction based on a specific range of intensity values from the defined volume. Figure S2 (C) illustrates this approach, which also highlights the difficulties associated with this method. In this example, the isosurface had to be created from a lower density volume than the original data set, since the original data resolution was too high to extract a surface in an acceptable time frame. Yet, the resulting surface description consists of about 1 million polygons that fail to capture the fine details of the original file. Furthermore, due to the

thresholding process during isosurface extraction, all volumetric information, including transparency and color gradients, are lost. Through the conversion process, the initial volumetric information is compromised and the generated model does not preserve the original internal volumetric details.

The STL files created by the two examples above would then be further processed by the 3D printer software, which slices the incoming STL files, determines the inside of the objects, and creates material deposition instructions for the printer hardware. Overall, the described conversion workflows result in computational overhead and alter the original data in a way that can generate discrepancies between the virtual and the physical visualization.

Post-Processing of 3D Printed Parts

The 3D printing systems used in our work make use of a support material (SUP705) to stabilize objects while they are being printed. The support material is removed after the print has been completed, resulting in surface roughness at the interface where the support material connects with the actual model material. For transparent materials, this may result in partially diminished optical clarity. However, since this is merely a surface effect, optical transparency can be fully restored by polishing and lacquering the 3D printed part with a clear coat.

Supplementary Figures

Limitations of Boundary Representations in 3D Printing Workflows

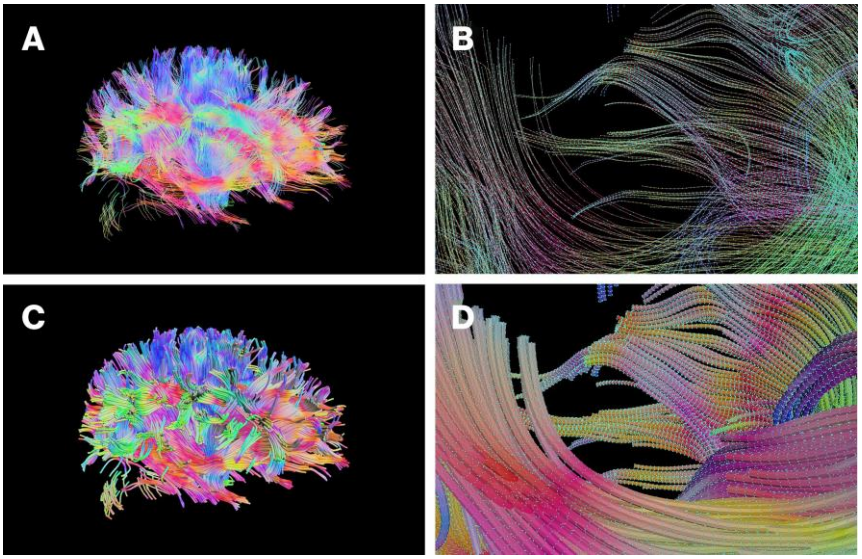

fig. S1. White matter tractography data, created with the 3D Slicer medical image processing platform (*37*). The whole data set consists of 5,721 fibers represented as polygon chains. (**A**)(**B**) The fiber data are represented as lines consisting of 625,078 vertices. (**C**)(**D**) In order to prepare the data set for conventional 3D printing processes, the fibers are converted into tubes that are now represented through a total of 6,250,780 vertices, which is an increase of the vertex count by a factor of 10.

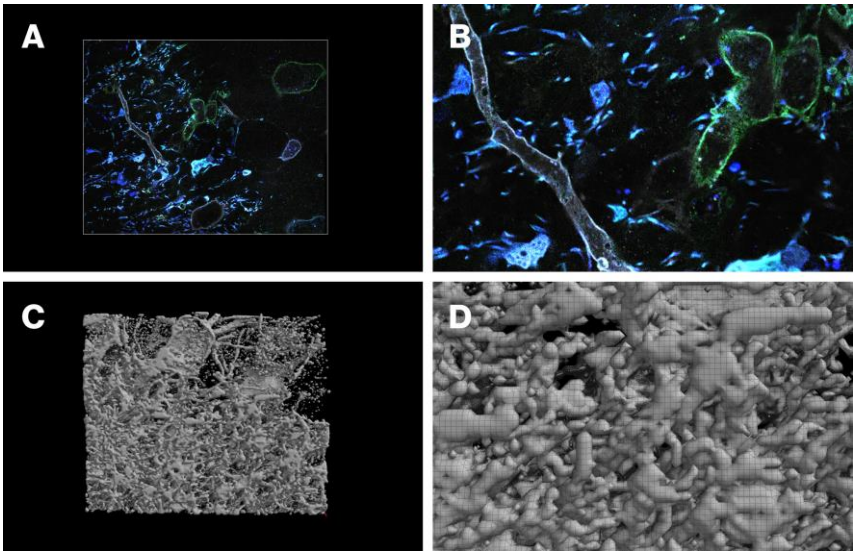

fig. S2. Image stack that captures data observed through protein-retention expansion microscopy (*30*). (**A**) and (**B**) show one slice of the image stack and a magnification thereof that together demonstrate the high level of detail stored in the data set. (**C**) shows an isosurface created from the whole image stack. As seen in the magnification of the data set (**D**), it is difficult to represent the information from the image stack as a 3D isosurface in any meaningful manner. Due to the nature of the conversion process, volumetric information and detail is lost.

Evaluation of Printable Features

fig. S3. Variability in optical transparency as a function of transparent opaque resin mixing ratios and feature size. (**A**) Line elements with a diameter range of 1.0 mm – 0.01 mm were 3D printed within transparent enclosures with mixing ratios of (left) 0% transparent (fully opaque) and 90% transparent material (right). All fully opaque lines are visible, while the lines with 90% transparent material content are visible only when the diameter is equal to or bigger than 0.3 mm. The dots shown in (**B**) exhibit similar behavior, where opaque dots with a diameter of 0.5 mm are clearly visible, while more transparent dots are only clearly perceivable at larger sizes. (**C**) shows a magnified view of the printed objects with geometric elements printed with pure opaque material content. Even though the features are very small, a 0.1 mm dot on the left and 0.01 mm line on the right are still noticeable, which highlights the ability of our method to fabricate very fine features. All feature sizes were established by visual inspection (n=6).

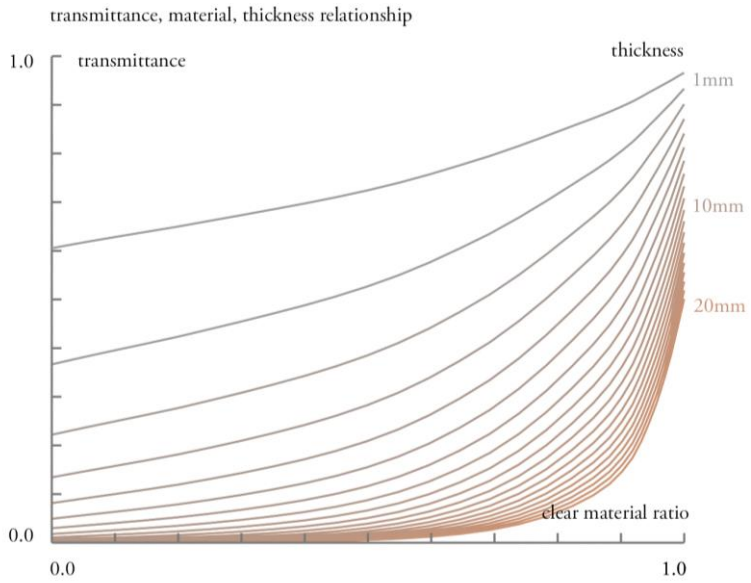

fig. S4. Transmittance behavior of material samples with different transparent-to-opaque material ratios. Transmittance was measured as ratio of transmitted light to incident light at 630 nm on 2 mm thick 3D printed samples. Twenty-nine samples were measured at six different positions. Homogenous transmittance behavior was assumed throughout a sample and therefore exponential transmittance falloff can be inferred by Beer-Lamberts law as the thickness of the sample increases. Assuming the transmittance is connected to perceptual translucency, this allows the nonlinear relationship between material-mixing ratios and perceived optical transparency to be inferred.

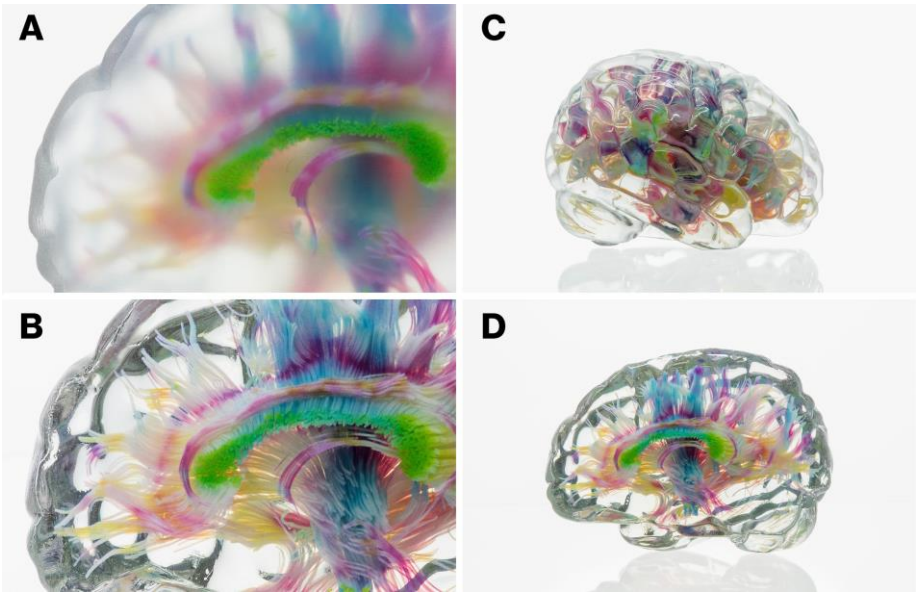

fig. S5. Two observed visual characteristics that arise from the use of the transparent build material. (**A**) 3D printed areas that were in contact with support material result in a matte finish. (**B**) Transparency can be easily restored through polishing and clear coat lacquering. (**C**) Curved surfaces like the brain folds refract light and hamper the view into the inside of the object. (**D**) However, flat surfaces like the cross-section of the brain, which is the back of the same model shown in (C) appear highly transparent and do not interfere with the data viewing.

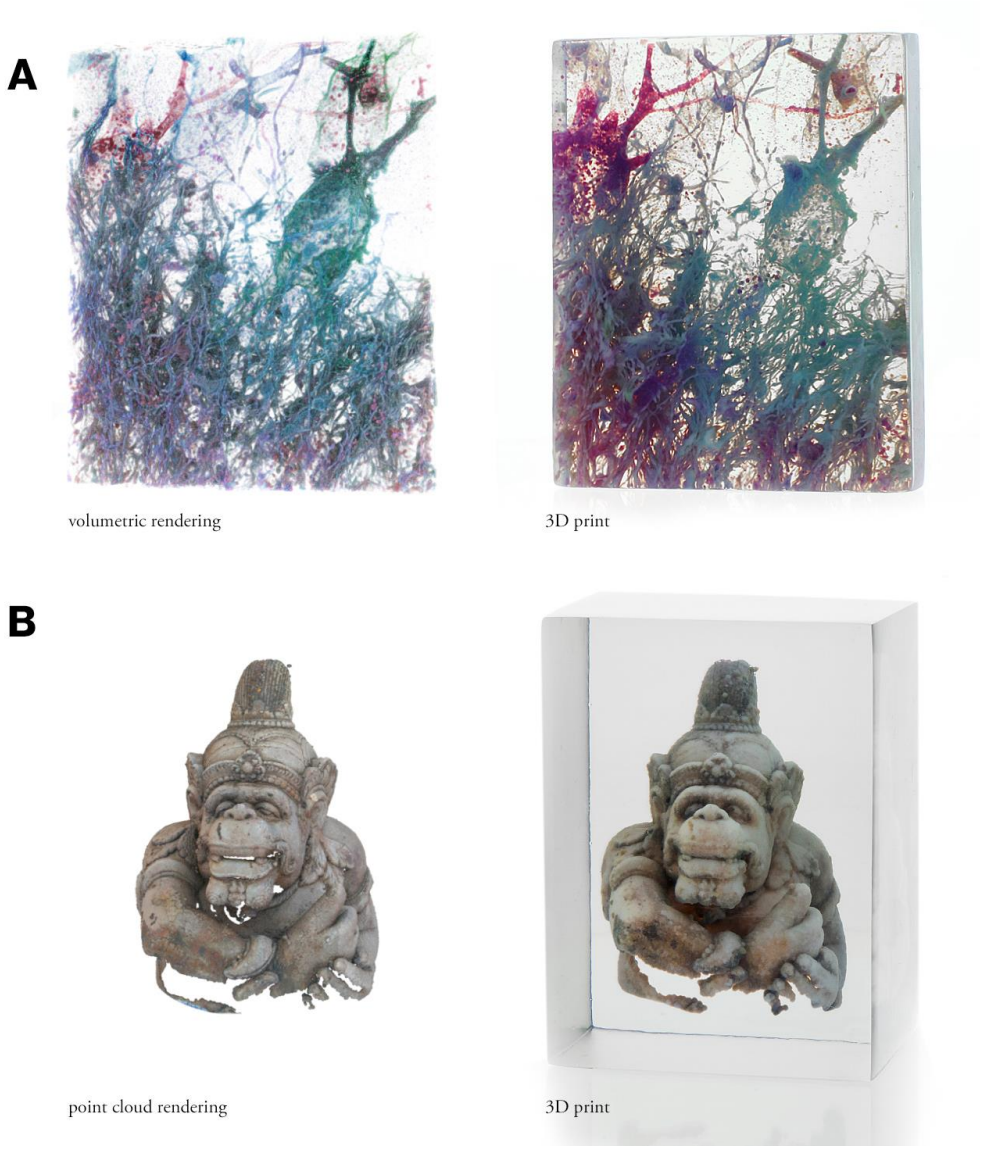

fig. S6. Comparison of 3D renderings to 3D-printed models produced with our method. (**A**) Digital volumetric visualization (on the left) compared to 3D-printed, physical visualization (on the right) of the image stack from Fig. 6 (B). For the visualization in (A), the image stack was converted to a volume of 54 million digital voxels. Through implementation of the introduced image-based voxel-printing process, the image stack was directly translated into a material volume of 1.1 billion individually addressable material voxels and the 3D-printed model result faithfully replicates the detail of the original digital rendering. (**B**) Point cloud rendering (on the left) compared to the 3D printed, physical visualization (on the right) of the point cloud from Fig. 3 (G). In this case, the diameter of the points can be adjusted in order to partially fill in gaps present in the original data (for example around the mouth and left hand of the statue).

Additional Examples

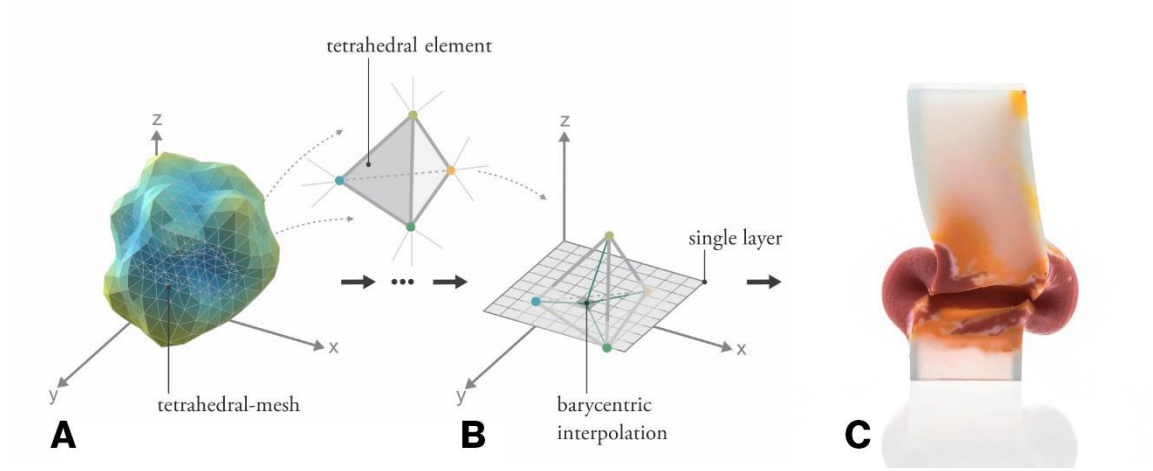

fig. S7. Brief illustration of the conversion of tetrahedral meshes to 3D printable models through our method. Brief description of the conversion of tetrahedral meshes (**A**) to 3D printable droplet depositing descriptions. For each layer, nodal data from the tetrahedral mesh intersecting with the material description layer is interpolated for each pixel occupied by a tetrahedron, through barycentric interpolation (**B**). An example is shown in (**C**). Here, a tetrahedral mesh of a simulation of the deformation of a compressed square tube through finite element methods is presented. High deformation is encoded as red opaque material and low deformation is encoded as partially transparent white material.

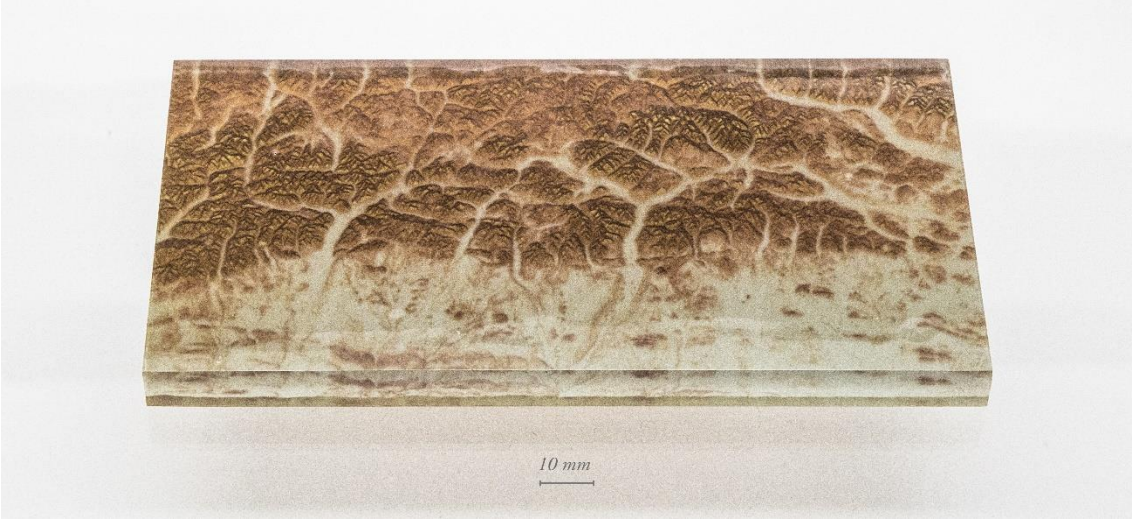

fig. S8. Elevation map of a portion of the Brooks Range in Northern Alaska. The data was obtained from the Elevation Derivatives for National Application (EDNA) database. The provided maps predict information such as slope, water flow accumulation, or flow direction within the elevation. Material voxels are vertically distributed as informed by the elevation map of the database. Each voxel is color-coded to reflect the degree of slope. Beige color indicates flat areas with low slope, whereas dark brown color indicates areas with high slope.